

Conducting Nanofibers and Organogels Derived from the Self-Assembly of Tetrathiafulvalene-Appended Dipeptides

Siva Krishna Mohan Nalluri,^{*,†} Nadezhda Shivarova,[‡] Alexander L. Kanibolotsky,[†] Mischa Zelzer,^{†,§} Swati Gupta,[‡] Pim W. J. M. Frederix,[†] Peter J. Skabar,[†] Helena Gleskova,^{*,‡} and Rein V. Ulijn^{*,†,‡,#}

[†]WestCHEM, Department of Pure & Applied Chemistry, University of Strathclyde, Glasgow G1 1XL, United Kingdom

[‡]Department of Electronic and Electrical Engineering, University of Strathclyde, Glasgow G1 1XW, United Kingdom

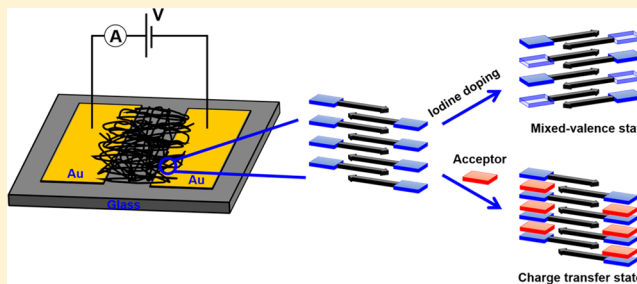
[§]Laboratory of Biophysics and Surface Analysis, School of Pharmacy, The University of Nottingham, Nottingham NG7 2RD, United Kingdom

[#]Advanced Science Research Center (ASRC), City University of New York, New York 10031, United States

[#]Department of Chemistry, Hunter College, City University of New York, New York 10065, United States

Supporting Information

ABSTRACT: We demonstrate the nonaqueous self-assembly of a low-molecular-mass organic gelator based on an electroactive p-type tetrathiafulvalene (TTF)-dipeptide bioconjugate. We show that a TTF moiety appended with diphenylalanine amide derivative (TTF-FF-NH₂) self-assembles into one-dimensional nanofibers that further lead to the formation of self-supporting organogels in chloroform and ethyl acetate. Upon doping of the gels with electron acceptors (TCNQ/iodine vapor), stable two-component charge transfer gels are produced in chloroform and ethyl acetate. These gels are characterized by various spectroscopy (UV-vis-NIR, FTIR, and CD), microscopy (AFM and TEM), rheology, and cyclic voltammetry techniques. Furthermore, conductivity measurements performed on TTF-FF-NH₂ xerogel nanofiber networks formed between gold electrodes on a glass surface indicate that these nanofibers show a remarkable enhancement in the conductivity after doping with TCNQ.



INTRODUCTION

There is significant current interest in the fabrication of functional organic nanomaterials based on electronically active π -conjugated chromophores, with diverse proposed applications in next-generation optoelectronic and bioelectronic devices.^{1–6} One challenge in this area is the difficulty in obtaining a high degree of organization among the constituent electroactive components, ultimately affecting the overall performance of the devices.⁷ The supramolecular assembly of π -conjugated chromophores into one-dimensional (1D) nanostructures with a high aspect ratio provides a potential strategy to tune the photonic/electronic properties as it facilitates the long-range intermolecular charge delocalization of π -electron cloud.^{8–10} In this respect, low-molecular-mass organic gelators (LMOGs) have attracted interest because of their ability to self-assemble into entangled three-dimensional (3D) fibrous network structures driven by multiple, weak intermolecular forces such as π – π stacking, van der Waals, electrostatic, metal coordination, charge transfer, and H-bonding interactions.^{11,12} A variety of supramolecular strategies have been developed to demonstrate the self-assembly of organogelators^{13–16} based on π -electron-deficient (n-type) aromatic building blocks, including naphthalene bisimides¹⁷ and perylene bisimides,^{18,19} as well as π -electron-rich (p-type)

aromatic building blocks, including triphenylenes,²⁰ oligo(*p*-phenylenevinylenes),²¹ oligothiophenes,²² porphyrins,²³ phthalocyanines,²⁴ merocyanines,²⁵ and tetrathiafulvalenes (TTFs).^{26–33} In particular, TTF-based LMOGs have been extensively investigated for the development of organic conducting nanomaterials^{27–30} and stimuli-responsive materials.^{26,31} It has been shown that TTF and its derivatives can form charge transfer complexes with various electron acceptors such as tetracyano-*p*-quinodimethane (TCNQ) and iodine, and the resultant charge transfer complexes exhibit high electrical conductivity.^{26,32,33}

One powerful strategy for the formation of highly organized π -conjugated LMOGs is focused on bioconjugates of π -conjugated chromophores and self-assembling peptides,^{34–36} in which the precise orientation and packing of the π -conjugated chromophores can be optimized by the intermolecular H-bonding of peptide motifs.^{37–40} In recent years, various functional organogels have been reported based on bioconjugates of peptides and ferrocene,⁴¹ azobenzene,⁴¹ stilbene,⁴² and pyrene.^{41,43} Supramolecular self-assembly of

Received: August 29, 2014

Revised: September 25, 2014

Published: September 26, 2014

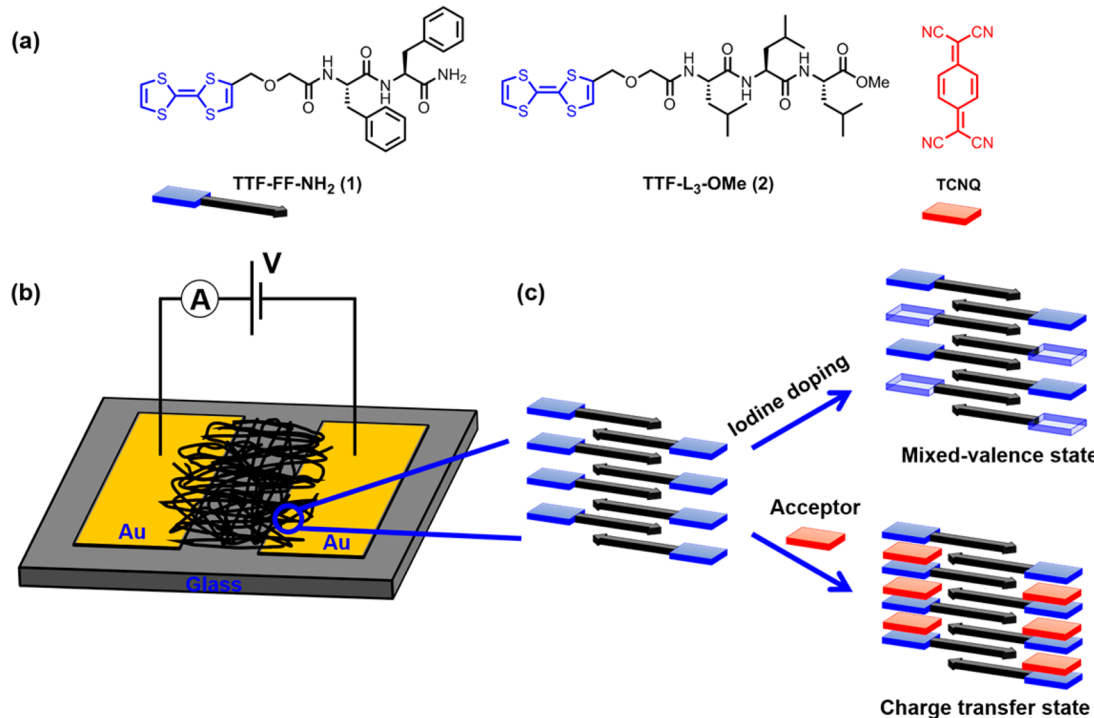


Figure 1. (a) Molecular structures of p-type TTF-peptide bioconjugates: TTF–diphenylalanine amide **1** (TTF-FF-NH₂) and TTF–trileucine methyl ester **2** (TTF-L₃-OMe) derivatives, and TCNQ acceptor used in this study. Schematic representation of (b) the method of electrical conductivity measurements of xerogel nanofiber networks drop-casted between gold electrodes on a sodium-free glass substrate and (c) the proposed mechanism of the nonaqueous self-assembly process of TTF–peptide bioconjugates and the formation of charge transfer and mixed-valence states upon doping with TCNQ and iodine, respectively.

bioconjugates of optoelectronically active (also including p- or n-type) π -conjugated chromophores and peptides in organic solvents have been reported.^{44,45} We have very recently reported the first example of fluorescent organogel based on bola-amphiphile type bioconjugates of n-type perylene bisimide and dipeptides.⁴⁶ However, this system forms gels only in high boiling point polar organic solvents such as DMF and DMSO and was not tested for electroconductance.⁴⁶ To the best of our knowledge, the conducting nanofibers and organogels derived from the self-assembly of TTF–peptide bioconjugates have not been reported, and such nanostructures have not been used to measure conductivity directly.^{5,32,47,48}

Herein, we investigate the supramolecular self-assembly of various bioconjugates of short peptides and TTF. For this purpose, we chose two types of functional TTF–peptide bioconjugates by simply varying the length and sequence of the peptide motifs present (Figure 1a). One is a TTF-appended aromatic dipeptide derivative **1** (TTF-FF-NH₂): that is, TTF moiety functionalized with a diphenylalanine amide derivative (FF-NH₂). The FF⁴⁹ sequence was selected as a suitable self-assembling peptide motif because it has been widely employed by us⁵⁰ and others^{49,51–55} previously. The other conjugate made use of an aliphatic tripeptide derivative **2** (TTF-L₃-OMe): that is, TTF moiety functionalized with a trileucine methyl ester derivative (L₃-OMe). The L₃ peptide sequence was selected based on our previous results using 9-fluorenylmethoxycarbonyl (Fmoc) peptides.^{47,56} The self-assembly of these bioconjugates is driven by the π – π stacking of TTF moieties as well as the intermolecular H-bonding of peptide motifs (Figure 1). The primary objectives of this work are (i) characterization of nanostructures formed in non-aqueous media using various spectroscopy, microscopy, and

rheology techniques, (ii) investigation of the effect of the presence of charge transfer interactions between TTF and TCNQ/iodine vapor on self-assembling electroactive nanostructures, and finally (iii) measurement of the electrical conductivity of electroactive xerogel networks formed both in the absence and presence of charge transfer in ambient air at room temperature (Figure 1).

EXPERIMENTAL SECTION

Materials. All commercial reagents were used as supplied. The compounds 7,7,8,8-tetracyanoquinodimethane (TCNQ) and iron(III) perchlorate hydrate (Fe(ClO₄)₃·H₂O) were purchased from Sigma-Aldrich (UK). All solvents were used as supplied (analytical or HPLC grade) without further purification, unless otherwise mentioned.

Synthesis. The TTF–peptide bioconjugates **1** and **2** were synthesized as reported in the Supporting Information. All reactions were carried out in oven-dried glassware and magnetically stirred. Thin layer chromatography (TLC) was performed on Merck silica gel 60 F254 plates. All compounds were visualized either by UV light source (254 nm) or by dipping in basic permanganate solution. Column chromatography was carried out by using silica gel 60 (230–400 mesh). High-resolution mass spectra (ESI-HRMS) were recorded on a Thermo Electron Exactive. ¹H and ¹³C nuclear magnetic resonance (NMR) spectra were recorded on Bruker AV400 spectrometer in the deuterated solvents. All chemical shifts (δ) are quoted in ppm, and coupling constants (J) are given in Hz. Residual signals from the solvents were used as an internal reference.

Gelation Experiments. The TTF-FF-NH₂ gelator (11.7 mg, 20 mM) was mixed in a particular organic solvent (1 mL) taken in a screw-capped sample vial. The mixture was vortexed followed by sonication for few seconds and heated until the solid was completely dissolved. The sample vial was cooled to room temperature and left for at least few hours under ambient conditions. Gelation was considered to have occurred when a homogeneous solid-like material was

obtained that exhibited no gravitational flow. In the case of chloroform, gelation was observed at 30 min after cooling to room temperature. Samples were incubated at room temperature for at least 12 h before further characterization, unless otherwise stated. In the case of charge transfer donor–acceptor organogels, both TTF-FF-NH₂ donor (2.93 mg) and TCNQ acceptor (1.02 mg) were mixed together in 250 μL of the solvent (chloroform/ethyl acetate) taken in a screw-capped vial. The self-supporting organogels were also obtained in this case by following the above procedure. The organogels were then characterized after equilibration for few hours under ambient conditions. The similar gelation tests were also performed on TTF-L₃-OMe (12.9 mg, 20 mM) by adding to a particular organic solvent (1 mL). The results are summarized in Table S1 of the Supporting Information.

UV–Vis Absorption Spectroscopy. UV–vis absorption spectra were recorded on a Jasco V-660 spectrophotometer. Samples were prepared in quartz cuvettes with 1 cm path length. The absorbance of TTF-FF-NH₂ solution in chloroform was measured in the absence and presence of TCNQ. The total chromophore concentration is 5 mM in this case.

UV–Vis–NIR Absorption Spectroscopy. UV–vis–NIR absorption spectra were recorded on a Shimadzu UV-2600 spectrophotometer with integrating sphere attachment ISR-2600 Plus equipped with two detectors (photomultiplier and InGaAs detector). The measurable wavelength range was 220–1400 nm. The gel sample in chloroform (20 mM) was prepared by depositing the hot solution of TTF-FF-NH₂ inside a quartz cuvette with 1 cm path length, and the cuvette was placed horizontally. After about 30 min, the solution was then developed into a self-supporting organogel on the sidewall of the quartz cuvette. The absorbance of this xerogel (dried for 30 min) was measured from 220 to 1400 nm. After doping with iodine by exposing the sample cuvette to iodine vapor for 50 min in a sealed container with iodine crystals (~10 mg), the absorbance of the gel was measured again. The appearance of a new absorption band near 850 nm accompanied by an increase in the absorbance indicated the formation of cation radical species and the corresponding mixed-valence states over time, which led to a change in color of the gel from yellow to dark brown.

Oscillatory Rheology. The mechanical properties of the organogels were investigated by dynamic frequency sweep experiments which were carried out by a strain-controlled rheometer (Kinexus Pro Rheometer) by employing parallel plates of 20 mm diameter with 0.5 mm gap. The experiments were performed at 20 °C, and this temperature was controlled throughout the experiment using an integrated electrical heater. Additional precautions were taken to minimize solvent evaporation and to keep the sample hydrated: a solvent trap was used and the internal atmosphere was kept saturated. To ensure the measurements were made in the linear viscoelastic regime, an amplitude sweep was performed, and the results showed no variation in elastic modulus (G') and viscous modulus (G'') up to a strain of 1%. The dynamic modulus of the gels was measured as a frequency function, where the frequency sweeps were carried out between 0.1 and 100 Hz. The measurements were repeated three times to ensure reproducibility, with the average data shown.

Fourier Transform Infrared (FTIR) Spectroscopy. FTIR spectra were recorded on a Bruker optics Vertex 70 spectrophotometer. The spectra were taken in the region between 800 and 4000 cm^{-1} with a resolution of 1 cm^{-1} and averaged over 20 scans. Spectra were background-subtracted to correct for atmospheric interference. For all measurements, the nondeuterated solvents (Sigma-Aldrich, UK) were used directly. The organogels were loaded between two CaF₂ windows using a 5 μm PTFE spacer. The spectra were recorded at 24 h after cooling the heated solution to room temperature under ambient conditions. For xerogel doping measurements, the instrument was used in attenuated total reflectance (ATR) mode. The gel sample in chloroform was allowed to dry on the diamond crystal, after which the spectra were taken. Samples were doped by placing I₂ crystals next to the dried sample and covering the sample with a beaker for 2 min, after which the beaker and I₂ were removed.

Circular Dichroism (CD). CD spectra were measured on a Jasco J600 spectropolarimeter in a 0.1 mm path length cylindrical cell, with 1 s integration, step resolution of 1 mm, response of 0.5 s with a bandwidth of 1 nm and slit width of 1 mm. The freshly prepared samples (hot solution) were directly added to the cell using a pipet, and the spectra were recorded after equilibration for 24 h. The high tension (HT) voltage values reach maximum below the wavelengths of 250 nm due to the high extinction coefficient of these semiconductor chromophores under these conditions, and the CD spectra could not be recorded in this wavelength region.

Atomic Force Microscopy (AFM). For AFM experiments, 20 μL of sample solution (as a gel/sol) was drop-casted onto a freshly cleaved mica surface (G250-2 mica sheets 1 in. × 1 in. × 0.006 in.; Agar Scientific Ltd, Essex, UK). Each sample was air-dried overnight in a dust-free environment prior to AFM imaging. For comparison, the sample solution was also drop-casted for AFM imaging on gold-coated glass surfaces used for electrical conductivity measurements. The images were obtained by scanning the mica/glass surfaces in air under ambient conditions using a Veeco diINNOVA scanning probe microscope (VEECO/BRUKER, Santa Barbara, CA) operated in tapping mode. The AFM measurements were obtained using sharp silicon probes (RTESPA; Veeco Instruments SAS, Dourdan, France). AFM scans were taken at 512 × 512 pixels resolution and produced topographic images of the samples in which the brightness of features increases as a function of height. Typical scanning parameters were as follows: tapping frequency 326 kHz, integral and proportional gains 0.1 and 0.3, respectively, set point 0.5–0.7 V, and scanning speed 1.0 Hz. AFM images were collected from two different samples and at random spot surface sampling (at least five areas). The images were analyzed using NanoScope Analysis software version 1.40.

Transmission Electron Microscopy (TEM). Transmission electron microscopy (TEM) images were captured using a LEO 912 energy filtering transmission electron microscope operating at 120 kV fitted with 14 bit/2 K Proscan CCD camera. Carbon-coated copper grids (200 mesh) were glow discharged in air for 30 s. The support film was touched onto the gel surface for 3 s and blotted down using filter paper. Negative stain (20 μL, 1% aqueous methylamine vanadate obtained from Nanovan, Nanoprobe) was applied, and the mixture was dried down again using filter paper. Each sample was allowed to dry afterward for a few minutes in a dust-free environment, and the dried specimens were then imaged using the microscope.

Cyclic Voltammetry (CV). Cyclic voltammetry (CV) measurements were performed on CH Instruments 660A electrochemical workstation with *iR* compensation using anhydrous chloroform as the solvent. The electrodes were platinum disk, platinum wire, and silver wire as the working, counter, and reference electrodes, respectively. All solutions contained substrates in concentrations of ca. 0.1 mM together with *n*-Bu₄NPF₆ (0.1 M) as the supporting electrolyte. The measurements are referenced against the $E_{1/2}$ of the Fc/Fc⁺ redox couple. The oxidation of the gel was performed by carefully inserting the platinum gauze (as a working electrode) into the gel phase.

Electrical Conductivity Measurements. Plane-parallel gold contacts were thermally evaporated on sodium-free glass substrates of 1 × 1 cm^2 with varying gap lengths of approximately 30, 50, 70, and 90 μm and a gap width of 1000 μm. The substrates were prepared by drop-casting the solution (either as a hot solution or after cooling the heated solution to room temperature) of TTF-FF-NH₂ (in chloroform) and left overnight under ambient conditions for structure formation and solvent evaporation. On the following day, the samples were placed in a vacuum chamber for an hour prior to the measurements. Similarly, the substrates doped with TCNQ were prepared by drop-casting the mixture of TTF-FF-NH₂ and TCNQ (1:1 ratio) in chloroform and left overnight under ambient conditions for structure formation and solvent evaporation, while the iodine doping was achieved by exposing the drop-casted TTF-FF-NH₂ substrates (without TCNQ) to iodine vapor for about 30 min in a sealed container with iodine crystals (~20 mg). The current–voltage (*I*–*V*) characteristics were measured in ambient air at room temperature using Signatone probe station and Agilent B1500A semiconductor parameter analyzer. The voltage was swept from 0 to

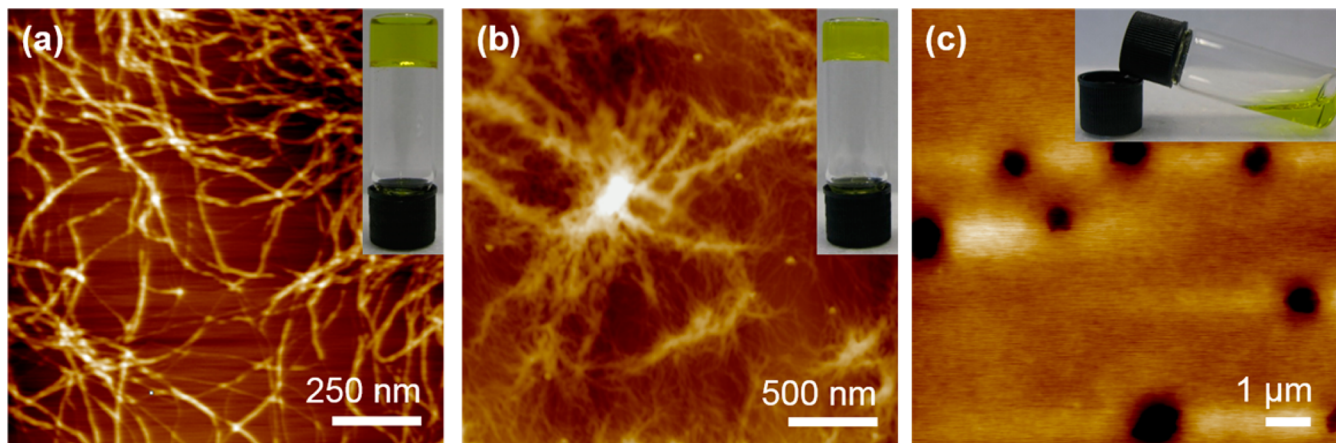


Figure 2. Tapping-mode AFM height images (on freshly cleaved mica) of dried samples of **1** in various organic solvents: (a) gel in chloroform, (b) gel in ethyl acetate, and (c) solution in tetrahydrofuran. Insets in (a–c) show the digital photographs the corresponding gel/sol samples.

20 V and in some cases up to 100 V. Temperature-dependent measurements were achieved by placing the sample on a thermoelectric heater/cooler in an in-house built stainless steel chamber connected to Agilent B1500A semiconductor parameter analyzer. The temperature of the Peltier element was controlled by an electric circuit with thermistor feedback via LabVIEW. The spring-loaded probes made electrical contact to the gold electrodes, and the measurements were taken from 20 to \sim 80 °C. The leakage current of the measurement system was subtracted from the I – V measurement of the samples. Two sets of samples were measured to obtain the dark conductivity of the gels of **1** in chloroform before and after doping with TCNQ/iodine.

RESULTS AND DISCUSSION

The syntheses of **1** and **2** were carried out by the condensation of TTF-substituted carboxylic acids and the corresponding free amine derivatives of diphenylalanine amide (FF-NH₂) and trileucine methyl ester (L₃-OMe). Details of the synthesis and characterization are reported in the Supporting Information. The analytical and spectroscopic data for **1** and **2** are fully consistent with their molecular structures. At first, the gelling abilities of both compounds **1** and **2** were tested in a number of common organic solvents. Typically, the compound (**1** or **2**) at 20 mM concentration was taken in an organic solvent and sequentially vortexed, sonicated, and heated until the solid was dissolved completely and left to stand at room temperature for few hours under ambient conditions. It was observed that **1** formed self-supporting yellow organogels particularly in chloroform (transparent gel formed within 30 min), ethyl acetate (slightly opaque gel formed within 2–3 h), and acetone (opaque gel formed within 2–3 h), which are stable in the gel state for several months. Formation of the gel in acetone required sonication for a few minutes before cooling the hot solution of **1** to room temperature, while direct cooling of hot solution without sonication led to precipitation and no gel was formed. Similar observations were reported elsewhere.^{26,57} Tetrahydrofuran, methanol, and DMSO were found to be good solvents for **1**, while it was found to precipitate in acetonitrile, cyclohexane, and benzene. The observations suggest differential self-assembly of **1** in various solvents which is likely to be dependent on the balance between intermolecular π – π stacking of the hydrophobic TTF units and the H-bonding of diphenylalanine peptide motifs, similar to what was observed for perylene bisimide-appended peptides.⁴⁶

In contrast, gelation was not observed for compound **2**, as it was either completely soluble or precipitated in these common organic solvents under ambient conditions. A complete list of solvents tested for **1** and **2** is summarized in Table S1 of the Supporting Information. The contrasting behavior of **1** and **2** can be reasonably explained by the fact that the presence of both aromatic (instead of aliphatic for **2**) and terminal free amide (instead of methyl ester for **2**) groups in the peptide backbone of **1** give rise to additional π – π stacking interactions combined with the extended H-bonding, offering a vital contribution to the overall thermodynamic stability of aggregates of **1** compared to the amorphous aggregates of **2**. Therefore, only the self-assembly of **1** was then studied in more detail.

We first focused on the morphological investigation of **1** in different solvents, e.g., chloroform, ethyl acetate, and tetrahydrofuran, by atomic force microscopy (AFM) as well as transmission electron microscopy (TEM). Tapping-mode AFM imaging of dried chloroform and ethyl acetate gel samples of **1** on mica revealed the formation of a dense network of entangled nanofibers of up to several micrometers in length (Figure 2a,b). The difference in transparency of the gels in various solvents (transparent, slightly opaque, and opaque gels in chloroform, ethyl acetate, and acetone, respectively) is due to the variation in the solubility with respect to temperature and assembly kinetics combined with the network properties of the nanofibers obtained. Also, TEM imaging of negatively stained (1% aqueous methylamine vanadate as a staining agent) dried gel samples of **1** in chloroform (on carbon-coated copper grid) similarly revealed the presence of micrometer-long nanofibers (Figure S1 in the Supporting Information). In contrast, both AFM (Figure 2c) and TEM (see Figure S1 in the Supporting Information) images of solution of **1** in tetrahydrofuran showed the presence of vesicles with variable diameters. It is noteworthy that the self-assembly of **1** into vesicles (instead of nanofibers) which lack the ability to generate a cross-linked network further explains the nongelation behavior of **1** in tetrahydrofuran. We then turned our attention to investigate the self-assembly behavior of **1** only in chloroform in further details, owing to its transparent gel nature and rapid self-assembly behavior compared to ethyl acetate system.

Having established the stable self-assembling nanofibers of **1** in chloroform, the ability to form the charge transfer complex within the π -stacked TTF assemblies of **1** was further

investigated. This can be approached in two ways. One approach is the partial oxidation of TTF moieties (giving rise to a mixed-valence state) which can be done either electrochemically or chemically, while the other approach is the chemical doping of the gels with electron acceptors such as TCNQ and iodine vapor. In order to investigate the first approach, the electrochemical properties of TTF moiety of **1** in chloroform were first analyzed by cyclic voltammetry that displayed two quasi-reversible one-electron oxidation waves in which the first oxidation at ca. $E_{1/2} = +0.04$ V (vs Fc/Fc⁺) and the second oxidation at ca. $E_{1/2} = +0.35$ V (vs Fc/Fc⁺) occurred which correspond to the formation of TTF radical cation (TTF^{•+}) and TTF dication (TTF²⁺) species, respectively (Figure S2 in the Supporting Information). The electrochemical oxidation of TTF moiety of gel **1** in chloroform (20 mM) was also observed by applying an oxidation potential of +0.8 V for about 30 min and after which the gel was transformed into a dark brown-green suspension (Figure 3a). As reported previously,²⁶ such a

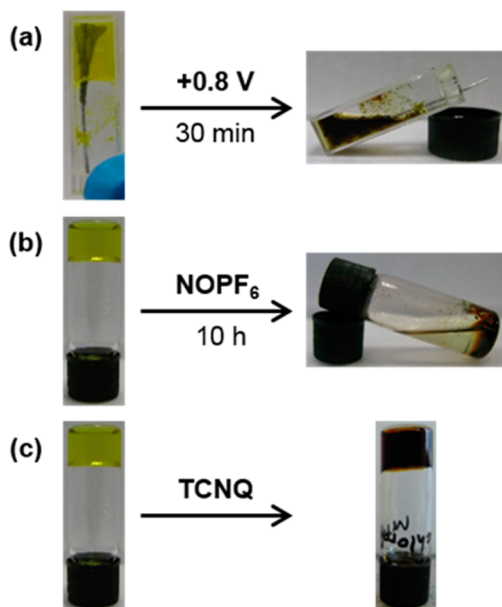


Figure 3. Digital photographs showing the different ways of achieving the charge transfer complex formation in gel of **1** in chloroform: that is by using (a) electrochemical oxidation, (b) chemical oxidation with NOPF₆, and (c) chemical doping with TCNQ. The quartz cuvette in (a) shows the inserted platinum gauze (used as a working electrode) into the sample.

relatively low first oxidation potential can be achieved by chemical oxidizing agents such as iron(III) perchlorate ((Fe(ClO₄)₃) and nitrosonium hexafluorophosphate (NOPF₆). In this context, we examined the state of gel of **1** in chloroform by carefully adding NOPF₆ on top of the gel surface and observed that the transparent yellow gel was destroyed gradually leading to a dark brown suspension within 2 h that eventually precipitates after about 10 h (Figure 3b).

These findings prompted us to evaluate the chemical doping capability of gels and further investigate the subsequent formation of charge transfer complexes in the gel phase of TTF donors with various electron acceptors such as TCNQ and iodine vapor. We first mixed **1** with TCNQ in chloroform in a 1:1 ratio. Upon cooling of the heated solution, a dark brown gel was observed (Figure 3c). The significant change in color of the gel from yellow (without TCNQ) to dark brown

(with TCNQ) is an indicative of the formation of a charge transfer complex (TTF^{•+}/TCNQ⁻) between TTF of **1** and TCNQ moieties. This charge transfer complex formation was further confirmed by UV-vis absorption spectroscopy. As shown in Figure 4a, the appearance of new absorption bands centered at 748, 850 nm in chloroform correspond to the formation of TCNQ radical anion species (TCNQ⁻)³³ and the increase in the absorbance in 600–700 nm region corresponds to the formation of TTF radical cation species (TTF^{•+}).⁵⁸ The presence of both these characteristic radical anion/cation species further confirmed the formation of charge transfer complex between TTF of **1** and TCNQ. This is an added advantage to the present system when compared to the previously reported systems on organogelators composed of modified TTF derivatives (1,4-dithiol ring fused TTF²⁶ and monopyrrolo-annulated TTF³³), where it was shown that the gel was destroyed upon the addition of TCNQ, caused by the electrostatic repulsions between positively charged TTF units (TTF^{•+}/TTF²⁺) would possibly impair the intermolecular H-bonding of adjacent urea/amide groups (instead of dipeptides), in polar organic solvents such as 1,2-dichloroethane²⁶ and ethanol.³³ All these observations clearly indicate that stable two-component charge transfer gels can be developed by doping the gel of **1** with TCNQ even in polar organic solvents.⁵⁹

We then characterized the gel of **1** in chloroform and further investigated the effect of charge transfer interactions on the gel network after doping with 1 equiv of TCNQ. The frequency-sweep measurements by oscillatory rheology for gel of **1** in chloroform at 20 °C indicated that the storage modulus G' is significantly higher than the loss modulus G'', confirming the viscoelastic behavior of the gel. The stiffness was found to be about 27 kPa (Figure 4b). Interestingly, the doping of gel of **1** with TCNQ slightly enhanced the stiffness up to 34 kPa (Figure 4b), indicative of the charge transfer complexation between TFF and TCNQ moieties. Furthermore, the morphological investigation of the TCNQ doped charge transfer gels in chloroform was carried out by tapping-mode AFM which clearly disclosed the development of a dense network of entangled nanofibers of up to several micrometers in length (Figure 4c). These results remarkably suggest that the charge transfer nanofibers of **1** were formed after doping with TCNQ, giving rise to the possibility of long-range charge delocalization of π-π associated TTF and TCNQ moieties along the length of the nanostructures.

The supramolecular interaction governing the self-assembly of bioconjugate **1** in chloroform before and after doping with TCNQ was further evaluated. There is a likely role of H-bonding involved in the self-assembly of **1** which was investigated by FTIR spectroscopy. H-bonding contributions for the formation of secondary structures were investigated by monitoring the absorption of gel of **1** in the amide I region. The spectrum of gel of **1** in chloroform showed strong amide I band at 1645 cm⁻¹, a characteristic band for the formation of aggregated intermolecular β-sheet-like secondary structures in chloroform (Figure 4d).^{28,45} Additionally, the presence of another strong band at 1670 cm⁻¹ corresponds to the hydrogen bonding of free terminal CONH₂ amide groups present in **1**. Furthermore, the formation of charge transfer complex (TTF^{•+}/TCNQ⁻) in TCNQ doped gel of **1** in chloroform was confirmed by the presence of TCNQ radical anion (TCNQ⁻) peak at 2182 cm⁻¹ in addition to TCNQ neutral peak at 2223 cm⁻¹ (a characteristic peak for the charge transfer complex-

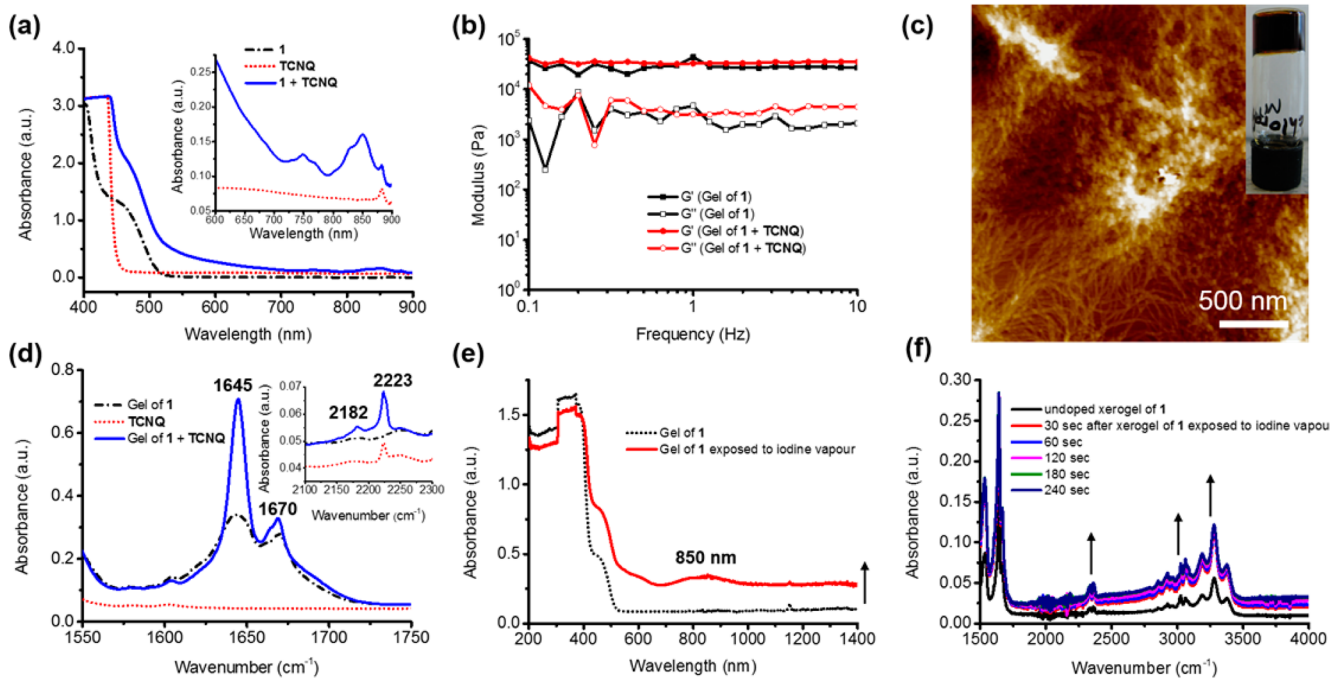


Figure 4. Self-assembly of bioconjugate **1** in chloroform before and after doping with TCNQ/iodine vapor. (a) UV-vis absorption spectra confirming the formation of two-component charge transfer complex between TTF of **1** and TCNQ. (b) Stiffness of gels of **1** before and after doping with TCNQ, as measured by oscillatory rheology. (c) Tapping-mode AFM image of charge transfer gel of **1** after doping with TCNQ. The inset shows the digital photograph of TCNQ doped charge transfer gel of **1**. (d) The amide I region of the FTIR spectra of gel of **1** showing the formation of intermolecular β -sheet-like H-bonding before and after doping with TCNQ. The spectra in the inset shows the changes in CN stretching frequency region of TCNQ. (e) UV-vis-NIR absorption spectra showing the charge transfer complex formation upon exposing the gel of **1** to iodine vapor in a sealed container. (f) FTIR spectra monitored over time after exposing the xerogel of **1** to iodine vapor in a sealed container. The time was monitored after removing the iodine crystals placed next to the xerogel sample.

ation),³³ while the solution of TCNQ in chloroform showed only TCNQ neutral peak at 2224 cm^{-1} (Figure 4d). The spectra of TCNQ doped charge transfer gel of **1** also showed a dramatic enhancement in the peak at 1645 cm^{-1} which is significantly dominating the peak at 1670 cm^{-1} , indicating the formation of reinforced intermolecular β -sheet-like H-bonding network (Figure 4d). CD spectroscopy was further used to investigate the relative intermolecular orientations of TTF units within the self-assembled nanostructures that give rise to specific CD signals emerging from the helical supramolecular orientation (rather than from the inherent molecular chirality) of the self-assembling building blocks. Notably, the CD spectrum of gel of **1** in chloroform displayed excitonic Cotton effects centered at approximately 285, 346, and 383 nm which correspond to $\pi-\pi^*$ transition peaks originated due to the helical orientation of TTF units (Figure S4).^{30,60} All spectroscopy, microscopy, and rheology results consistently indicate that the presence of additional charge transfer interactions within the self-assembled nanostructures, thereby perhaps allowing the more ordered coassembly of TTF donors of **1** and TCNQ acceptors, gives rise to the formation of reinforced charge transfer gels likely with better conducting pathways along the length of the nanofibers.⁴⁰

Similarly, such charge transfer complexation within the stacked TTF assemblies of **1** can also be obtained by doping with iodine. The UV-vis-NIR and FTIR spectroscopy techniques were employed to confirm the charge transfer complexation on xerogel networks (surface dried films) of **1** upon exposed to iodine vapor in a sealed container. To this end, we prepared the gel samples of **1** in chloroform on the sidewall of a quartz cuvette, dried for 30 min, and exposed the

xerogel sample to iodine vapor for 50 min. The corresponding UV-vis-NIR absorption spectra of the doped gel sample in Figure 4e revealed the appearance of a broad absorption band at around 850 nm , which is a characteristic band for the formation of a complete charge transfer state between dimeric cation radical species of stacked TTF units (TTF^+I^-). Additionally, the significant increase in the absorbance in the higher wavelength region ($>600\text{ nm}$) indicates the formation of a more conducting partial charge transfer (mixed-valence) state between neutral and cation radical species of TTF moieties ($(\text{TTF})(\text{I})_n$, where $n < 1$) within the stacked TTF assemblies of **1**.³² Also, the charge transfer complex formation in the xerogel networks of **1** upon exposing to iodine vapor for 2 min was successfully confirmed by the significant increase in the absorbance over time above 1700 cm^{-1} region in the FTIR spectra (Figure 4f), indicating the formation of a mixed-valence state within the stacked TTF assemblies of xerogel of **1**.³²

The electrical conductivity of nanofibers obtained by xerogel samples of **1** from chloroform was further measured. The conductivity measurements were performed by drop-casting the gel samples between gold electrodes deposited on a sodium-free glass surface. All measurements for undoped and doped xerogel samples of **1** showed approximately linear $I-V$ characteristics (Figure 5a). This indicates Ohmic rather than rectifying contacts. The conductivity of the xerogel of **1** was calculated as follows

$$R = \rho \frac{L}{dW} = \frac{1}{\sigma} \frac{L}{dW} = \frac{1}{G} \quad (1)$$

where R is resistance of the xerogel film, ρ is its resistivity, L is the length of the gap between gold contacts, d is the thickness

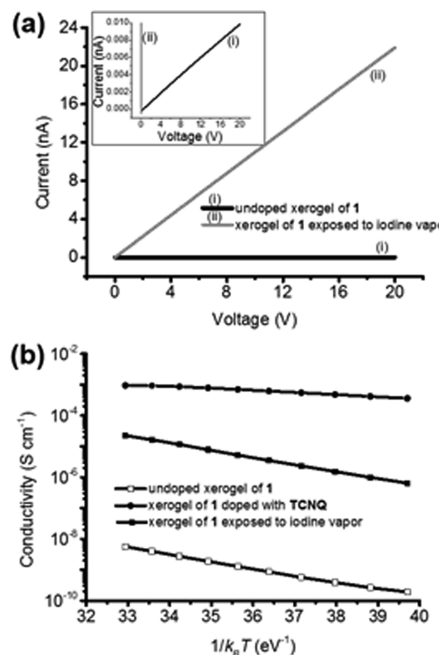


Figure 5. (a) Current–voltage (*I*–*V*) characteristics and (b) the temperature-dependent conductivity measurements of the xerogels of **1** (obtained from chloroform) before and after doping with TCNQ/iodine vapor.

of the film, *W* is the width of the gold contacts, σ is the conductivity of the film, and *G* is its conductance. From this, it can be seen that

$$\sigma = G \frac{L}{dW} \quad (2)$$

The dark conductivity was measured as a function of temperature between 20 and 80 °C for both undoped and iodine doped xerogel samples of **1** obtained from chloroform and fitted with the following exponential dependence

$$\sigma = \sigma_0 \exp\left(\frac{-E_a}{k_B T}\right) \quad (3)$$

where *T* is the absolute temperature, k_B is the Boltzmann constant, E_a is the activation energy of the conductivity, and σ_0 is the conductivity prefactor. The activation energy E_a can be found as the slope of the straight line on a semilogarithmic plot of the conductivity versus the reciprocal thermal energy. Whether band theory for structurally ordered materials, tight-binding models for weakly disordered systems, or hopping models for localized charges in strongly disordered materials are employed, the activation energy represents the energy barrier for the drifting charge carriers to reach the transport level or hop to the neighboring electronic site.

The conductivity of the undoped xerogel of **1** shown in Figure 5b was $\sigma_{20\text{ }^\circ\text{C}} = 1.9 \times 10^{-10} \text{ S cm}^{-1}$ (typically behaving as undoped semiconductor), and the activation energy was $E_a = 0.67 \text{ eV}$. Interestingly, the conductivity of xerogel of **1** doped with TCNQ remarkably enhanced to $\sigma_{20\text{ }^\circ\text{C}} = 3.6 \times 10^{-4} \text{ S cm}^{-1}$ and the activation energy was $E_a = 0.18 \text{ eV}$. However, the conductivity of xerogel of **1** after iodine doping (30 min) was only increased to $\sigma_{20\text{ }^\circ\text{C}} = 6.4 \times 10^{-7} \text{ S cm}^{-1}$ (more conducting behavior in the charge transfer state), and the corresponding activation energy was $E_a = 0.53 \text{ eV}$. In particular, the remarkable enhancement in the conductivity for TCNQ doped xerogels is

likely to depend on the strong intermolecular charge transfer interactions between TTF and TCNQ moieties as well as the length of stacks obtained. The $\sigma_{20\text{ }^\circ\text{C}}$ of four samples of the undoped xerogel of **1** with varied *L* and *d* was the same within $\pm 17\%$, while the E_a showed standard deviation of $\pm 0.07 \text{ eV}$. After doping with TCNQ/iodine, $\sigma_{20\text{ }^\circ\text{C}}$ values fell within $\pm 35\text{--}45\%$, while E_a exhibited smaller standard deviation of $\pm 0.03 \text{ eV}$. Given the fibrous morphology of the xerogel samples of **1** (Figures 2a and 4c), some deviations are expected. Better connectivity of the densely populated nanofiber areas would lead to higher conductivity. In addition, since the nanofibers exhibit random orientation (Figures 2a and 4c), the effect of the direction of the applied electric field should be insignificant.

The increase in the conductivity upon TCNQ/iodine doping of xerogel samples of **1** indicated the formation of a more conducting charge transfer state (Figures 4e,f), resulting in the increased conductivity prefactor. The significant reduction in the activation energy after TCNQ doping of xerogel samples of **1** suggests tighter packing of the TTF moieties due to strong charge transfer interactions between TTF and TCNQ moieties. Additionally, the temperature dependent conductivity measurements between 20 and 80 °C reveal an exponential dependence of conductivity on temperature which is typical for semiconductor materials. Interestingly, our observations are similar to the values reported by Kitamura et al., where it was shown that the conductivity of the nanofiber networks composed of a TTF moiety functionalized with L-isoleucine in aromatic liquid crystals (instead of common organic solvents) exhibit ca. $3 \times 10^{-10} \text{ S cm}^{-1}$ when undoped and $2 \times 10^{-7} \text{ S cm}^{-1}$ after iodine doping for 2 min which was further increased to $3 \times 10^{-5} \text{ S cm}^{-1}$ after 1 week, while the doping of fibers with TCNQ increased the conductivity to $1 \times 10^{-5} \text{ S cm}^{-1}$.³² All these results consistently indicate that the two-component charge transfer nanofibers of TTF–dipeptide bioconjugates, formed upon doping with TCNQ/iodine vapor, exhibit good conductivity and clearly behave as semiconducting nanomaterials.

CONCLUSIONS

In summary, we successfully demonstrated the supramolecular self-assembly of p-type TTF-dipeptide bioconjugates into 1D nanofibers that further lead to the development of self-supporting gels in common organic solvents such as chloroform and ethyl acetate. It was also shown that the gels in chloroform (or ethyl acetate) can be doped with TCNQ/iodine vapor to form stable two-component charge transfer gels. The charge transfer complexation was further confirmed by various spectroscopy, microscopy, and rheology techniques. Moreover, the investigation of the conductivity of the nanofiber xerogel networks formed between gold electrodes on a glass surface showed a remarkable enhancement in the conductivity from 1.9×10^{-10} (undoped) to $3.6 \times 10^{-4} \text{ S cm}^{-1}$ when doped with TCNQ and $6.4 \times 10^{-7} \text{ S cm}^{-1}$ when exposed to iodine vapor. This approach certainly provides potential opportunities for the bottom-up fabrication of cost-effective functional biomaterials that may find applications in interfacing biology with electronic devices such as organic and bioinspired solar cells, smart biomaterials, and biosensors.

ASSOCIATED CONTENT

S Supporting Information

Synthesis and experimental details, additional spectroscopy and microscopy results, and copies of ¹H and ¹³C nuclear magnetic

resonance (NMR) spectra. This material is available free of charge via the Internet at <http://pubs.acs.org>.

AUTHOR INFORMATION

Corresponding Authors

*E-mail siva.nalluri@strath.ac.uk (S.K.M.N.).
*E-mail helena.gleskova@strath.ac.uk (H.G.).
*E-mail rein.ulijn@strath.ac.uk (R.V.U.).

Notes

The authors declare no competing financial interest.

ACKNOWLEDGMENTS

The research leading to these results has received funding from US Air Force (AFOSR, grant no. 12448RK7359A) and EPSRC. The authors thank Conor Moynihan, Joanna Sobon, Jan Čermák, and Dr. A. R. Inigo for their assistance. We also thank Margaret Mullin from University of Glasgow for help in TEM imaging.

REFERENCES

- (1) Schenning, A. P. H. J.; Meijer, E. W. Supramolecular Electronics; Nanowires from Self-Assembled π -conjugated systems. *Chem. Commun.* **2005**, 3245–3258.
- (2) Hirst, A. R.; Escuder, B.; Miravet, J. F.; Smith, D. K. High-Tech Applications of Self-Assembling Supramolecular Nanostructured Gel-Phase Materials: From Regenerative Medicine to Electronic Devices. *Angew. Chem., Int. Ed.* **2008**, 47, 8002–8018.
- (3) Aida, T.; Meijer, E.; Stupp, S. Functional Supramolecular Polymers. *Science* **2012**, 335, 813–817.
- (4) Busseron, E.; Ruff, Y.; Moulin, E.; Giuseppone, N. Supramolecular Self-Assemblies As Functional Nanomaterials. *Nanoscale* **2013**, 5, 7098–7140.
- (5) Babu, S. S.; Praveen, V. K.; Ajayaghosh, A. Functional π -Gelators and Their Applications. *Chem. Rev.* **2014**, 114, 1973–2129.
- (6) Santhosh Babu, S.; Aimi, J.; Ozawa, H.; Shirahata, N.; Saeki, A.; Seki, S.; Ajayaghosh, A.; Möhwald, H.; Nakanishi, T. Solvent-Free Luminescent Organic Liquids. *Angew. Chem., Int. Ed.* **2012**, 51, 3391–3395.
- (7) Cademartiri, L.; Ozin, G. A. Ultrathin Nanowires—A Materials Chemistry Perspective. *Adv. Mater.* **2009**, 21, 1013–1020.
- (8) Hoeben, F. J. M.; Jonkheijm, P.; Meijer, E. W.; Schenning, A. P. H. J. About Supramolecular Assemblies of π -Conjugated Systems. *Chem. Rev.* **2005**, 105, 1491–1546.
- (9) Zang, L.; Che, Y.; Moore, J. S. One-Dimensional Self-Assembly of Planar π -Conjugated Molecules: Adaptable Building Blocks for Organic Nanodevices. *Acc. Chem. Res.* **2008**, 41, 1596–1608.
- (10) Das, A.; Ghosh, S. Supramolecular Assemblies by Charge-Transfer Interactions between Donor and Acceptor Chromophores. *Angew. Chem., Int. Ed.* **2014**, 53, 2038–2054.
- (11) Terech, P.; Weiss, R. G. Low Molecular Mass Gelators of Organic Liquids and the Properties of Their Gels. *Chem. Rev.* **1997**, 97, 3133–3160.
- (12) Notably, the functional LMOGs have many advantages when compared to the conventional gels such as electroactive polymer gels (in general, the gelators require cumbersome synthesis and obtained in less yields combined with the poor solubility in aqueous/organic media) and supramolecular hydrogels (in general, the gelators based on electroactive π -conjugated chromophores have poor aqueous solubility and the presence of ions/buffer hinders the conductivity measurements).
- (13) Babu, S. S.; Prasanthkumar, S.; Ajayaghosh, A. Self-Assembled Gelators for Organic Electronics. *Angew. Chem., Int. Ed.* **2012**, 51, 1766–1776.
- (14) Prasanthkumar, S.; Saeki, A.; Seki, S.; Ajayaghosh, A. Solution Phase Epitaxial Self-Assembly and High Charge-Carrier Mobility Nanofibers of Semiconducting Molecular Gelators. *J. Am. Chem. Soc.* **2010**, 132, 8866–8867.
- (15) Garcia, F.; Buendia, J.; Ghosh, S.; Ajayaghosh, A.; Sanchez, L. Luminescent and Conductive Supramolecular Polymers Obtained from an N-Annulated Perylenedicarboxamide. *Chem. Commun.* **2013**, 49, 9278–9280.
- (16) Prasanthkumar, S.; Gopal, A.; Ajayaghosh, A. Self-Assembly of Thienylenevinylene Molecular Wires to Semiconducting Gels with Doped Metallic Conductivity. *J. Am. Chem. Soc.* **2010**, 132, 13206–13207.
- (17) Mukhopadhyay, P.; Fujita, N.; Takada, A.; Kishida, T.; Shirakawa, M.; Shinkai, S. Regulation of a Real-Time Self-Healing Process in Organogel Tissues by Molecular Adhesives. *Angew. Chem., Int. Ed.* **2010**, 49, 6338–6342.
- (18) Sugiyasu, K.; Fujita, N.; Shinkai, S. Visible-Light-Harvesting Organogel Composed of Cholesterol-Based Perylene Derivatives. *Angew. Chem., Int. Ed.* **2004**, 43, 1229–1233.
- (19) Draper, E. R.; Walsh, J. J.; McDonald, T. O.; Zwijnenburg, M. A.; Cameron, P. J.; Cowan, A. J.; Adams, D. J. Air-Stable Photoconductive Films Formed from Perylene Bisimide Gelators. *J. Mater. Chem. C* **2014**, 2, 5570–5575.
- (20) Hirai, Y.; Monobe, H.; Mizoshita, N.; Moriyama, M.; Hanabusa, K.; Shimizu, Y.; Kato, T. Enhanced Hole-Transporting Behavior of Discotic Liquid-Crystalline Physical Gels. *Adv. Funct. Mater.* **2008**, 18, 1668–1675.
- (21) Ajayaghosh, A.; Praveen, V. K. π -Organogels of Self-Assembled p-Phenylenevinylenes: Soft Materials with Distinct Size, Shape, and Functions. *Acc. Chem. Res.* **2007**, 40, 644–656.
- (22) Schoonbeek, F. S.; van Esch, J. H.; Wegewijs, B.; Rep, D. B. A.; de Haas, M. P.; Klapwijk, T. M.; Kellogg, R. M.; Feringa, B. L. Efficient Intermolecular Charge Transport in Self-Assembled Fibers of Mono- and Bithiophene Bisurea Compounds. *Angew. Chem., Int. Ed.* **1999**, 38, 1393–1397.
- (23) Shirakawa, M.; Fujita, N.; Shinkai, S. A Stable Single Piece of Unimolecularly π -Stacked Porphyrin Aggregate in a Thixotropic Low Molecular Weight Gel: A One-Dimensional Molecular Template for Polydiacetylene Wiring up to Several Tens of Micrometers in Length. *J. Am. Chem. Soc.* **2005**, 127, 4164–4165.
- (24) Engelkamp, H.; Middelbeek, S.; Nolte, R. J. M. Self-Assembly of Disk-Shaped Molecules to Coiled-Coil Aggregates with Tunable Helicity. *Science* **1999**, 284, 785–788.
- (25) Yao, S.; Beginn, U.; Gress, T.; Lysetska, M.; Würthner, F. Supramolecular Polymerization and Gel Formation of Bis-(merocyanine) Dyes Driven by Dipolar Aggregation. *J. Am. Chem. Soc.* **2004**, 126, 8336–8348.
- (26) Wang, C.; Zhang, D.; Zhu, D. A Low-Molecular-Mass Gelator with an Electroactive Tetrathiafulvalene Group: Tuning the Gel Formation by Charge-Transfer Interaction and Oxidation. *J. Am. Chem. Soc.* **2005**, 127, 16372–16373.
- (27) Akutagawa, T.; Kakiuchi, K.; Hasegawa, T.; Noro, S.-i.; Nakamura, T.; Hasegawa, H.; Mashiko, S.; Becher, J. Molecularly Assembled Nanostructures of a Redox-Active Organogelator. *Angew. Chem., Int. Ed.* **2005**, 44, 7283–7287.
- (28) Puigmartí-Luis, J.; Laukhin, V.; Pérez del Pino, Á.; Vidal-Gancedo, J.; Rovira, C.; Laukhina, E.; Amabilino, D. B. Supramolecular Conducting Nanowires from Organogels. *Angew. Chem., Int. Ed.* **2007**, 46, 238–241.
- (29) Puigmartí-Luis, J.; Pérez del Pino, Á.; Laukhina, E.; Esquena, J.; Laukhin, V.; Rovira, C.; Vidal-Gancedo, J.; Kanaras, A. G.; Nichols, R. J.; Brust, M.; Amabilino, D. B. Shaping Supramolecular Nanofibers with Nanoparticles Forming Complementary Hydrogen Bonds. *Angew. Chem., Int. Ed.* **2008**, 47, 1861–1865.
- (30) Tatewaki, Y.; Hatanaka, T.; Tsunashima, R.; Nakamura, T.; Kimura, M.; Shirai, H. Conductive Nanoscopic Fibrous Assemblies Containing Helical Tetrathiafulvalene Stacks. *Chem.—Asian J.* **2009**, 4, 1474–1479.
- (31) Wang, C.; Chen, Q.; Sun, F.; Zhang, D.; Zhang, G.; Huang, Y.; Zhao, R.; Zhu, D. Multistimuli Responsive Organogels Based on a New Gelator Featuring Tetrathiafulvalene and Azobenzene Groups: Reversible Tuning of the Gel–Sol Transition by Redox Reactions and Light Irradiation. *J. Am. Chem. Soc.* **2010**, 132, 3092–3096.

- (32) Kitamura, T.; Nakaso, S.; Mizoshita, N.; Tochigi, Y.; Shimomura, T.; Moriyama, M.; Ito, K.; Kato, T. Electroactive Supramolecular Self-Assembled Fibers Composed of Doped Tetraphiafulvalene-Based Gelators. *J. Am. Chem. Soc.* **2005**, *127*, 14769–14775. This paper describes the first example of hydrogen-bonded conducting nanofibers based on the conjugates of p-type tetraphiafulvalene, amino acid (instead of peptides), and a long hydrocarbon chain. However, this system could form gels only in aromatic liquid crystals but not in common organic solvents at room temperature.
- (33) Liu, Y.; Zheng, N.; Li, H.; Yin, B. Supramolecular Gels Based on Monopyrrolotetraphiafulvalene and Its TCNQ Charge-Transfer Complex. *Soft Matter* **2013**, *9*, 5261–5269.
- (34) Zhang, S. Fabrication of Novel Biomaterials through Molecular Self-Assembly. *Nat. Biotechnol.* **2003**, *21*, 1171–1178.
- (35) Boyle, A. L.; Woolfson, D. N. De Novo Designed Peptides for Biological Applications. *Chem. Soc. Rev.* **2011**, *40*, 4295–4306.
- (36) Fichman, G.; Gazit, E. Self-Assembly of Short Peptides to Form Hydrogels: Design of Building Blocks, Physical Properties and Technological Applications. *Acta Biomater.* **2014**, *10*, 1671–1682.
- (37) Kim, S. H.; Parquette, J. R. A Model for the Controlled Assembly of Semiconductor Peptides. *Nanoscale* **2012**, *4*, 6940–6947.
- (38) Nalluri, S. K. M.; Ulijn, R. V. Discovery of Energy Transfer Nanostructures Using Gelation-Driven Dynamic Combinatorial Libraries. *Chem. Sci.* **2013**, *4*, 3699–3705.
- (39) Sahoo, J. K.; Nalluri, S. K. M.; Javid, N.; Webb, H.; Ulijn, R. V. Biocatalytic Amide Condensation and Gelation Controlled by Light. *Chem. Commun.* **2014**, *50*, 5462–5464.
- (40) Nalluri, S. K. M.; Berdugo, C.; Javid, N.; Frederix, P. W. J. M.; Ulijn, R. V. Biocatalytic Self-Assembly of Supramolecular Charge-Transfer Nanostructures Based on n-Type Semiconductor-Appended Peptides. *Angew. Chem., Int. Ed.* **2014**, *53*, 5882–5887.
- (41) Afrasiabi, R.; Kraatz, H.-B. Small-Peptide-Based Organogel Kit: Towards the Development of Multicomponent Self-Sorting Organogels. *Chem.—Eur. J.* **2013**, *19*, 15862–15871.
- (42) Maiti, D. K.; Banerjee, A. A Synthetic Amino Acid Residue Containing A New Oligopeptide-Based Photosensitive Fluorescent Organogel. *Chem.—Asian J.* **2013**, *8*, 113–120.
- (43) Adhikari, B.; Nanda, J.; Banerjee, A. Pyrene-Containing Peptide-Based Fluorescent Organogels: Inclusion of Graphene into the Organogel. *Chem.—Eur. J.* **2011**, *17*, 11488–11496.
- (44) Schillinger, E.-K.; Mena-Osteritz, E.; Hentschel, J.; Börner, H. G.; Bäuerle, P. Oligothiophene Versus β -Sheet Peptide: Synthesis and Self-Assembly of an Organic Semiconductor-Peptide Hybrid. *Adv. Mater.* **2009**, *21*, 1562–1567.
- (45) Jahnke, E.; Weiss, J.; Neuhaus, S.; Hoheisel, T. N.; Frauenrath, H. Synthesis of Diacetylene-Containing Peptide Building Blocks and Amphiphiles, Their Self-Assembly and Topochemical Polymerization in Organic Solvents. *Chem.—Eur. J.* **2009**, *15*, 388–404.
- (46) Bai, S.; Debnath, S.; Javid, N.; Frederix, P. W. J. M.; Fleming, S.; Pappas, C.; Ulijn, R. V. Differential Self-Assembly and Tunable Emission of Aromatic Peptide Bola-Amphiphiles Containing Perylene Bisimide in Polar Solvents Including Water. *Langmuir* **2014**, *30*, 7576–7584.
- (47) Xu, H.; Das, A. K.; Horie, M.; Shaik, M. S.; Smith, A. M.; Luo, Y.; Lu, X.; Collins, R.; Liem, S. Y.; Song, A.; Popelier, P. L. A.; Turner, M. L.; Xiao, P.; Kinloch, I. A.; Ulijn, R. V. An Investigation of the Conductivity of Peptide Nanotube Networks Prepared by Enzyme-Triggered Self-Assembly. *Nanoscale* **2010**, *2*, 960–966.
- (48) Torres, E.; Puigmarti-Luis, J.; Perez del Pino, A.; Ortuno, R. M.; Amabilino, D. B. Use of Unnatural β -Peptides as a Self-Assembling Component in Functional Organic Fibres. *Org. Biomol. Chem.* **2010**, *8*, 1661–1665.
- (49) Reches, M.; Gazit, E. Casting Metal Nanowires Within Discrete Self-Assembled Peptide Nanotubes. *Science* **2003**, *300*, 625–627.
- (50) Smith, A. M.; Williams, R. J.; Tang, C.; Coppo, P.; Collins, R. F.; Turner, M. L.; Saiani, A.; Ulijn, R. V. Fmoc-Diphenylalanine Self Assembles to a Hydrogel via a Novel Architecture Based on π – π Interlocked β -Sheets. *Adv. Mater.* **2008**, *20*, 37–41.
- (51) Reches, M.; Gazit, E. Controlled Patterning of Aligned Self-Assembled Peptide Nanotubes. *Nat. Nanotechnol.* **2006**, *1*, 195–200.
- (52) Yan, X.; Cui, Y.; He, Q.; Wang, K.; Li, J. Organogels Based on Self-Assembly of Diphenylalanine Peptide and Their Application To Immobilize Quantum Dots. *Chem. Mater.* **2008**, *20*, 1522–1526.
- (53) Yan, X.; Zhu, P.; Li, J. Self-Assembly and Application of Diphenylalanine-Based Nanostructures. *Chem. Soc. Rev.* **2010**, *39*, 1877–1890.
- (54) Adler-Abramovich, L.; Kol, N.; Yanai, I.; Barlam, D.; Shneck, R. Z.; Gazit, E.; Rouso, I. Self-Assembled Organic Nanostructures with Metallic-Like Stiffness. *Angew. Chem., Int. Ed.* **2010**, *49*, 9939–9942.
- (55) Erdogan, H.; Sakalak, H.; Yavuz, M. S.; Demirel, G. Laser-Triggered Degelation Control of Gold Nanoparticle Embedded Peptide Organogels. *Langmuir* **2013**, *29*, 6975–6982.
- (56) Williams, R. J.; Smith, A. M.; Collins, R.; Hodson, N.; Das, A. K.; Ulijn, R. V. Enzyme-Assisted Self-Assembly under Thermodynamic Control. *Nat. Nanotechnol.* **2009**, *4*, 19–24.
- (57) Cravotto, G.; Cintas, P. Molecular Self-Assembly and Patterning Induced by Sound Waves. The Case of Gelation. *Chem. Soc. Rev.* **2009**, *38*, 2684–2697.
- (58) Jain, A.; Rao, K. V.; Mogera, U.; Sagade, A. A.; George, S. J. Dynamic Self-Assembly of Charge-Transfer Nanofibers of Tetraphiafulvalene Derivatives with F(4)TCNQ. *Chem.—Eur. J.* **2011**, *17*, 12355–12361.
- (59) The similar two-component charge transfer gels of **1** doped with TCNQ were also observed in ethyl acetate which was further confirmed by the clear change in color of the gel, UV-vis absorption spectroscopy, and AFM (Figure S3 in the Supporting Information).
- (60) The CD data of TCNQ doped charge transfer gel of **1** in chloroform could not be obtained as the corresponding HT voltage data reached maximum values within the measured wavelength region.